Multi-scale experimental investigations of the thermal degradation of pine needles

T. Fateh [a*], F. Richard [b], J. Zaida [b], T. Rogaume [b] and P. Joseph[c].

a) FireSERT, School of the Built Environment and the Built Environment Research Institute, Ulster University, Newtownabbey, BT37 0QB, United kingdom.

b) Institut Pprime, CNRS (UPR-3346), Université de Poitiers, ISAE-ENSMA, F86961 Futuroscope, France.

c) Centre for Environmental Safety and Risk Engineering, Victoria University, PO Box 14428, Melbourne 8001, Australia.

* Corresponding author: Phone: +44 (0) 2890368766

Fax: (+44) (0)28 90368726, Email: t.fateh@ulster.ac.uk

Abstract

In this work, the thermal degradation of pine needles (from a Mediterranean species) was studied using a thermo-gravimetric analyser (TGA) and cone calorimeter that were coupled to FTIR spectrometer. The thermo-gravimetric analyses were carried out at four heating rates, in both air and nitrogen atmospheres. The evolution of gaseous components, mass loss and mass loss rate were recorded as a function of time and temperature. In order to account for the observed behaviours of the materials, we have also proposed a mechanism for the thermal degradation of pine needles, by primarily analysing both the evolutions of mass loss rate and gaseous components under nitrogen and air atmospheres. The kinetic parameters were subsequently estimated by using a genetic algorithm method.

The cone calorimetric measurements were mainly conducted with a view to investigating the influence of thermal transfer processes, occurring in a porous bed of pine needles with regard to its thermal degradation. The experiments were conducted at five external heat fluxes under a well ventilated atmosphere. Measurements consisted of the mass loss, mass loss rate and the amount of gaseous emissions. The main gases emitted during the thermal degradation and the combustion of the pine needles were found to be CH_4, CO, CO_2, NO and water vapour. In addition, the evolution of the temperature was measured by using a set of five thermocouples, placed in a vertical position at the centreline of the sample. The results obtained showed that the bed of pine needles behaved as a thermally thick fuel. On the contrary at higher the external heat fluxes, the sample behaved as a thermally thin sample.

Keywords

Vegetation, Forest fire, Thermal decomposition, Cone calorimeter, Thermo-gravimetric analysis, Pyrolysis, Gaseous emissions, Kinetic model.

Nomenclature

A	Pre-exponential factor (s^{-1})	n	Reaction order
c_p	Specific heat capacity ($j.kg^{-1}.K$)	t	Time (s)
Ea	activation energy ($J.mol^{-1}$)	T	Temperature (°C)

K	Reaction rate constant (s^{-1})	β	Heating rate ($°C.min^{-1}$)
m	Mass (g)	$\dot{m}$	Mass flow loss rate ($g.s^{-1}$)
E	Huggett's constant ($MJ.kg^{-1}$)	TGA	Thermo-gravimetric analysis
MLR	Mass loss rate ($g.s^{-1}$)	R	Universal gas constant (8.3145 $j.mol^{-1}.k^{-1}$)
TML	Total mass loss (g)	δ	Factor (1 under air and 0 under nitrogen)
FPA	Fire propagation apparatus	DSC	Differential scanning calorimeter
i	Species	X_i	Mole fraction of species b in the exhaust gas measured by analyser
CHF	Critical Heat Flux ($kW.m^{-2}$)	FTIR	Fourier transformed infrared spectroscopy
M_i	Molecular weight ($g.mol^{-1}$)	V_m	Molar volume ($l.mol^{-1}$)
y_{O2}	Mass fraction of oxygen	HRR	Heat release rate ($kw.m^{-2}$)
k	Reaction number	y	Mass fraction of species
A	Sample area exposed to the heat flux (m^2)	*IR*	Infrared
PP	Pinus Pinaster	*AU*	Arbutus Unedo
EA	Erica Arborea	*CM*	Cistus Monspeliensis
MCT	Mercury Cadmium Telluride	V	Volume (m^3)
GA	Genetic algorithms	ϕ	Fitness
ω_i	Reaction rate	υ	Stoichiometric factor

1. INTRODUCTION

Over the past several years, a number of devastating fires around the Mediterranean area alone have destroyed hundreds of thousands of acres of forest land. As it stands, the average number of forest fires occurring annually throughout the Mediterranean basin amount to about 50,000 [1]. Furthermore, the annual cumulated burnt acreage in the Mediterranean area is estimated to be around 600,000 ha [1]. Therefore, given the frequency, intensity and ferocity of forest fires, these devastating events have led to significant damages to the flora and fauna of the affected areas and have thus resulted in a huge drainage of the public revenue. The fuel load that feeds forest fires can be complex in nature, with varied physio-chemical properties, and a clear understanding

of the degradation behaviours and combustion attributes of the primary fuels involved is crucial in tackling wildland fires.

The experimental investigation of each fire scenario is not an easy task given the fact that each fire is different, in terms of the intensity and duration of the ignition, the fuel load, and other environmental factors, such as temperature, humidity, wind etc. However, modelling efforts in this area is more promising as several approaches, such as empirical [2-3], semi-empirical [4] and physics-based [5] are available. Among these, the physics-based models have the added advantage that the overall phenomena are described in detail. Thus, several numerical simulation codes have been developed by the scientific community for this purpose. These models also require the knowledge of the thermal properties of materials, as well as the determination of the mechanism(s) of thermal degradation and the associated kinetic parameters [6-10]. Such empirical parameters are often determined from small-scale tests such as TGA, DSC [11-16] and through medium-scale experiments like the cone calorimetry [17-21].

Several studies are already reported in the literature on the thermal degradation of forest vegetation that utilize mg of samples in a thermogravimetric analyser (TGA), or in a differential scanning calorimeter (DSC) [11-16]. Although the degradation parameters are generally well monitored in these tests, the results obtained are not sufficient to be able to describe real fire situations, where the heating rates are much higher than the heating rates employed, especially during those small-scale tests. Moreover, the propagation of the fire and associated diffusive phenomena cannot be taken into account at a mg scale. Hence, the results obtained will not facilitate the determination of the rate of fire spread under different set conditions, as encountered in a typical forest fire (such as density of the fuel bed, wind, slope of the terrane, etc.).

In the past, some studies were also conducted using the cone calorimeter bench scale [18-22], or a similar apparatus such as the fire propagation apparatus (FPA) [23], with a view to understanding the general behaviours forest fuels in fires. However, questions still remain on the understanding of the fundamental physio-chemical processes underpinning the thermal degradation of the vegetation and its numerical representation. This mainly arises as these investigations were focused on the influence of several parameters (the vegetation nature, the

density, the fuel bed (porosity) and the air entrainment) on the wildland fuel ignition. Indeed, in order to gather reliable information, the underlying heat and mass transfer processes should be characterized in the porous bed and at the interface between the flame and the surface of the bed. Furthermore, these processes should be investigated through both numerical simulations and additional experiments involving appropriate instrumentation

It is relevant to note here that a review, published in 2002 [24], has demonstrated the emissions of gaseous species during wildland fires. The data primarily relates to the vegetation in USA in the context of wildfires and prescribed fires in forests and rangelands. Similarly, the Fire Paradox European project was set out to determine the importance of fuel dependent behaviour and other parameters affecting the combustion of forest fuels. This project also made recommendations regarding conducting future tests using smaller opening baskets and denser fuel beds [25].

Recently, using a laboratory-scale calorimetric experiment, a reported study [26] employed laboratory-cured samples with different moisture conditions (fresh or oven dry). The results showed that the least flammable samples were that of fresh live needles. It was also found that fresh live needles generally ignited about four times slower, and burned with ~60% lower power and ~50% lower heat of combustion than dead needles. Moreover, the CO/CO_2 ratios were 0.07, 0.15 and 0.02 for the fresh live, fresh aged and fresh dead fuel respectively. However, this work is of limited applicability as it only employed just one incident heat flux ($50kW.m^{-2}$).

Several models have also been proposed in the literature relating to others materials by employing one or multi reaction mechanistic steps [10, 19, 22-23, 27]. In these studies, the primary mechanism is determined according to the steps required to reproduce the evolution of the experimentally determined mass loss rate without having any correlation with the gaseous emissions during the thermal degradation of the material under consideration (at a mg scale in a TGA apparatus). However, it has been shown that the consideration of the gaseous emissions is of great importance [24-25].

In this context, the primary aim of the present paper is to characterize the thermal decomposition of typical vegetation involved into the forest fires, such as pine needles. The article is organized in the following way: firstly, information regarding the materials is given, followed by

experimental details. Secondly, the results and discussions concerning the thermal degradation, the gaseous emissions at different scales and a kinetic mechanism of thermal decomposition are presented. Subsequently, the conclusions from work are provided.

2. Experimental setup

Pine needles (Pinus Pinaster) were collected from the Mediterranean basin (city of Marseille-France) [28]. In order to investigate of thermal decomposition of the pine needles, a multi-scale approach is utilized, mainly based on experimental runs using a TGA apparatus (0-D at a small scale) followed by a cone calorimeter (1-D at a medium scale):

The elementary analysis results of the combustible material are presented in table 1. The density of pine needles was 630 $kg.m^{-3}$ and the emissivity is of 0.95 [28-29].

The degradation studies were performed on a TA-Instrument TGA Q50, with sample masses of about 5±1 mg and at four heating rates (5, 10, 15, 20 $°C.min^{-1}$) from the ambient temperature (20°C) to 1000°C, in air and nitrogen. The lowest heating rates (<20$°C.min^{-1}$) are chosen based on a review conducted by Torero [30], where it was shown that the output from TGA runs were independent of the heating rates at the lower values. The gaseous species released during the experiments were analysed using a FTIR spectrometer (Thermo-Nicolet 6700 equipped with a MCT-A detector) coupled to the outlet of TGA apparatus. IR spectra were recorded in the spectral range of 4000-650 cm^{-1} with a resolution of 4 cm^{-1} and were averaged over 16 scans [31-32].

At the medium scale, the experiments were conducted under ambient air and in a well-ventilated condition using a cone calorimeter (ISO 5660) [17, 33]. For each external heat flux, a minimum of five runs were done in order to ascertain the reproducibility of the results. The measurements were performed by putting the sample holder in a horizontal position under heat fluxes between 15 to 50 $kW.m^{-2}$. The test runs were stopped after 30 min if no ignition occurred [17], and at sustained flaming conditions, the time to ignition and the mass evolution were recorded for each sample.

A specific sample holder has been used in the present study which is shown in Figures 1 and 2. It consisted of a stainless steel basket that was open at the top, 12.0 cm in diameter and 7.0 cm in height. The basket was designed to insure the homogeneity of the external irradiance over the sample surface, and the current design was similar to the one reported elsewhere [23, 34]. The bottom of the basket was insulated with 2 cm of insulating material, and this condition resembled the practical situation where needles are deposited on the soil. The sample holder was filled consistently by the same experimenter with 14.2 g of pine needles in order to attain a fuel volume fraction of 0.04; this value being representative of Mediterranean forest litters [28-29].

The evolution of the temperature was measured in parallel by using five thermocouples (type K with a diameter of 1 mm) placed in a vertical position, as shown in Figure 2. The thermocouples (V_1 to V_5) were positioned along the centreline every 1 cm from the exposed surface up to the back surface of the sample.

3. Results and discussion

3.1. Thermo-gravimetric analysis

a) Results under nitrogen

Figure 3 presents the evolution of the mass of the solid material as a function of temperature under nitrogen for different heating rates. Therefore, the corresponding thermograms denote the degradation reactions under purely pyrolytic conditions. As can be seen from the figure 3, the mass loss curves evolutions are similar regardless of the value of the heating rate. It can be also noted that about 10% of the initial mass was degraded between the ambient temperature (20°C) and 200°C. Furthermore, about 40 % of the initial mass was found to be degraded between 200 and 400°C, while 20% of the initial mass was lost between 400°C and the end of the test (1000°C). The mass of residue left at the end of the test was about 25% of the initial mass of the sample regardless of the heating rate.

Figure 4 depicts the mass loss rate as a function of temperature at the different heating rates. In the initial stages, the moisture is released and the thermal degradation starts soon after (around 200°C) under all heating rates. All the peaks of MLR curves occur around the same temperature ranges regardless of the heating rates. An increase of the heating rate led to a rise in the intensity

of MLR and the curves were shifted to higher temperatures. This behaviour is a characteristic feature denoting the role of the heating rate alone on the thermal degradation behaviour of the material under consideration. We could also make the assumption that the change of the heating rate does not significantly affects the reactions and associated kinetic parameters. The overall thermal degradation profile can be classified along three temperature ranges as follows:

- Between 200 and 330-350°C (depending on the heating rate), the MLR increases with the rise of temperature.
- Between 330-350°C and 380-420°C (depending on the heating rate), the MLR increases sharply to attain the maximal value and then it decreases.
- Between 380-420°C (depending on the heating rate) to the end of the test, the MLR decreases very slowly and becomes insignificant.

Following on from the profiles of the MLR curves, we suppose four main reaction steps:

- Evaporation of the moisture: corresponding to the first peak of MLR
- Three pyrolytic processes: the first corresponding to the peak of MLR curve at around 300°C, the second corresponding to the highest peak of MLR at around 380°C and the last reaction corresponding to the last peak of MLR at around 420°C.

In order to complete the investigation of the thermal degradation, the gaseous emissions correlation studies were conducted. The combined TGA/FTIR analyses are very useful in this context as in the combined mode the technique will help to identify the gases evolved at different stages of pyrolysis. These gases have a direct bearing on the flammability attributes and toxicity characteristics of solid materials undergoing combustion reactions in a real fire scenario. Moreover, the following of the gaseous emissions gives important information about the thermal degradation process.

An example of the evolutions of the gaseous components detected under inert atmosphere as a function of the temperature (therefore, during purely thermal degradation) are plotted in Figure 5 for a heating rate of 10°C.min^{-1}. It should be noted here that the emissions obtained at this specific heating rate are representative of the corresponding ones at the other heating rates (i.e.

the compositional profiles of the gaseous components did not change with the change in heating rates).

The main gases observed are: water vapour, methane, carbon monoxide, carbon dioxide, acetic acid, ammonia, formic acid, methanol and an alkane. As can be also seen, the water is released in two steps. The moisture is released first, with a maximum value occurring at 105°C, but bound water molecules get released later on and are detected between 210 and 800°C, with a maximum value at around 390°C. The first peak is directly related to the evaporation step, but the second one is probably due to the main pyrolysis step (dehydration reactions) as it is correlated to the peak of MLR.

The carbon dioxide is released between 200°C and the end of test, with a maximum value at 390°C. The carbon monoxide is detected when the temperature is above 310°C, with a maximum value at 380°C. The release of CO occurs around the temperature at which the second step of pyrolysis reaction. As the CO_2 is produced at the lower temperatures, the second pyrolysis step could be a partial oxidation of char, when CO is produced (i.e. char + $CO_2 \rightarrow$ CO + residue). Formic acid is detected at 240°C and up to 400°C whereas acetic acid is observed in the range of 260–440 °C. In addition, the methane is observed at higher temperatures, between 350°C and 800°C, while the methanol is observed between 200 and 500°C. During the experiment, an alkane molecule is observed between the 300 and 600°C.

The evolution of the gaseous emissions seems to confirm that the thermal degradation of the pine needles under inert atmosphere takes place in three main steps.

b) Results under air

The thermal degradation of the pine has been studied under different heating rates, in air, in order to identify the influence of the oxygen on the thermal degradation mechanism. Figure 6 shows the evolution of the mass as a function of the temperature under air. As can be seen, the evolutions of the curves are quite similar whatever the value of heating rate. The main thermal degradation takes place between 200 and 650°C, and the following observations can also be noted:

- Between the ambient temperature and 200°C: about 10% of the initial mass is lost and this can be attributed to evaporation of the moisture from the sample.
- Between 200 and 350°C: 40% of the initial mass is lost.
- Between 350 and 500°C: 45% of initial mass is lost.
- Between 500 and 650°C: the mass lost is relatively small.
- After 650°C; the mass lost appears to be negligible.

At the end of the test, the residue represents about 5 % of the initial mass, whatever the chosen heating rate.

The influence of the oxygen on the thermal decomposition is depicted in Figure 7, which shows the evolution of the mass loss rates as a function of the temperature. The MLR profiles are quite similar regardless of the heating rate. However, an increase in heating rate generally leads to a rise of the intensity of MLR curve. Moreover, the temperature corresponding to the maximum intensity of the MLR increases with the rise of the heating rate as already noticed in Figure 4. As before, in the case of degradation under nitrogen atmosphere, the heating rate does not seem to change the reactions and associated kinetic parameters. Indeed, any changes in MLR curves seem to arise from the manner in which the sample is heated and not to any changes in the nature of the underlying reaction steps.

From the analysis of the evolutions of the MLR curves, the thermal degradation steps under air can be classified according to the following temperature ranges, as given below:

- Between the ambient to 200°C, this can be attributed to the evaporation of the moisture.
- Between 200 and 330-350°C (depending on the heating rate), the MLR increases with the rise of temperature.
- Between 330-350°C and 380-400°C (depending on the heating rate), the MLR decreases sharply.
- Between 380-400°C to 450-470°C (depending on the heating rate), the MLR rises gradually until to reach the maximal value.

- Between 450-470°C and 550°C (depending on the heating rate), firstly MLR decreases slightly and then levels of.
- Between 640-660°C (depending on the heating rate), a small peak of mass loss rate can be observed.

We have also attempted to correlate the evolution of the gaseous emissions to the MLR. Figure 8 shows the gases detected during the experiments, as well the evolution of MLR as a function of the temperature, at the specific heating rate of 10°C.min^{-1}. It can be noted here that the moisture is released first with a maximum value at 110°C, and in addition water vapour evolution is also observed between 250 and 550°C. Methane is observed between 350 and 550°C, whereas methanol is detected between 250 and 420°C. Furthermore, carbon monoxide is detected between 300 and 550°C and the carbon dioxide between 280 and 550°C. Other species included: formic acid detected in trace concentration; acetic acid in the range of 260–400°C; and the ammonia between 250 and 500°C. It can be also noted here that, at lower temperatures between 200°C and 400°C, methanol, acetic acid and formic acid were found to be oxidized in contrary to the case with the inert atmosphere. However, at higher temperatures, alkane molecules, once formed, appear to undergo oxidation through a different mechanism(s), as compared to those occurring in the case of the inert atmosphere. This is revealed by the lower intensities the corresponding peaks. The production of CO_2 at higher temperature (500°C) could be due to a third reaction corresponding to the oxidation of char.

From the analysis of both the evolution of the MLR and the gaseous emissions as a function of the heating rate, we formulate that the thermal degradation of the pine needles under air takes place in 3 steps. In comparison, the corresponding processes appear take place in four steps under nitrogen, thus indicating the influence of the nature of the prevailing atmosphere on the degradation of the material.

c) Influence of the nature of the atmosphere

Figures 9 and 10, which present a comparison of the evolution of the mass and mass loss rate respectively under nitrogen and air for a heating rate of 10°C.min^{-1}, help to illustrate the influence of oxygen in the degradation of pine needles.

It should be noted here that the general profiles of evolution of the gaseous species are not affected by the heating rate. The evolutions of the mass loss as well as the mass loss rate as a function of the temperature are quite similar when the temperature is less than 300°C in both atmospheres. However above 300°C, the presence of oxygen seems to significantly alter the curves, notably for temperatures higher than 400°C. In addition, the residue obtained at the end of the test under air is less than the one under nitrogen (about 22% of the initial mass was found to be consumed by oxidative reactions).

From the comparison of the evolution of the mass loss and the mass loss rate, and taking into account the gaseous emissions for different heating rate and atmosphere conditions, the following observations could be made:

- Initially, the moisture is released in both atmospheres.
- Between 200 and 280°C, the profiles of the mass loss and mass loss rate curves are quite similar for both atmospheres. During this temperature range, acetic acid, water vapour, ammonia, methanol, formic acid and CO_2 are detected, which also agrees with previous studies [35-38]. Given the striking similarity between the profiles of the curves, in both atmospheres, it can be concluded that the underpinning physio-chemical processes are also similar along this range. Therefore, the nature of the prevailing atmosphere does not seem to influence the degradative reactions.
- Between 280 and 350°C, the mass loss rate slightly increases in nitrogen, while in air, the mass loss rate increases more strongly. During this step, water, CO, ammonia, and CO_2 are detected. It can be also seen that even though the intensity of MLR curve under air is higher than that under nitrogen, the shapes are similar. Thus, under air, the reactions can be considered as occurring in parallel to those happening under N_2.
- Between 350 and 380°C, the MLR decreases strongly regardless of the atmosphere, and during this step, acetic acid, water, CO, and CO_2 are detected. Indeed, the alkane is detected under nitrogen while ammonia is detected under air. Thus, the some of the reactions under air can be considered to be occurring in parallel to those ones under N_2.
- Between 380 and 550°C, the MLR decreases slightly under nitrogen, while under air, it increases further before it sharply decreases. During this step CO and CO_2 are detected. Thus extra reactions seem to occur under air.

With respect to the thermal degradation of pine needles, under the two atmospheres, we could link the thermal degradation of each constituents of the material to the various steps in the overall degradation as follows:

The first step is clearly due to the removal of the moisture of the pine needle because only H_2O can be assumed to be released around 100°C, whereas the first step of pyrolysis (200 – 330/350°C) can be attributed to the degradation of the hemicelluloses and lignin components. Indeed, White and Dietenberger [35] showed that the hemicelluloses and lignin components are pyrolyzed in the temperature ranges 200-300°C and 225-450 °C, respectively. They also indicated that most of the acetic acid liberated from wood pyrolysis is attributed to deacetylation of hemicellulose. In this study, acetic acid is detected from 350°C to around 600°C which can be considered to be released through the degradation of the hemicellulose and lignin.

The second step of pyrolysis (between 330/350 – 380/420°C) seems to correspond to the degradation of cellulose. According to a previous study [35], the depolymerization of cellulose occurs in the temperature range 300-350°C.

The last step of pyrolysis could correspond to the end of reactions of lignin (380/420°C – to the end of the run). According to the literature precedent [35], the degradation reaction of lignin is exothermic in nature, with peaks occurring between 225°C and 450°C.

The dehydration reactions occurring around 200°C are primarily responsible for pyrolysis of hemicellulose and lignin, and results in a high char yield for wood. Although cellulose remains mostly unpyrolyzed, its thermal degradation can be accelerated in the presence of water, acids, and oxygen. The tar generally undergoes cracking to form lighter gases and depolymerization to char residues. The overall pyrolysis reactions are endothermic in nature due to decreasing dehydration and increasing CO formation resulting from the char reacting with H_2O and CO_2 with increasing temperatures. During this “low-temperature pathway” of pyrolysis, exothermic reactions of exposed char and volatiles with atmospheric oxygen are manifested as glowing combustion [35]. The first peak of MLR under air could be the result of the two processes mentioned above occurring during the range of temperatures under

consideration. According to previous paper [35], for temperatures higher than 450°C, the remaining wood can be considered as a char residue, which undergoes further degradation through oxidation reactions to form CO_2, CO, and H_2O vapour. This is often referred to as the afterglow. The last reactions of oxidation detected in this study is also char oxidation.

In conclusion, we can state that the first step occurs only under nitrogen while the second and the third steps occur under both atmospheres. The last step is facilitated by oxygen and thus occurs only under air.

Table 2 presents the decomposition mechanisms by taking into account of the fate and evolution of both solid and gas phases.

From the above analysis, the following reaction pathways can be formulated for pine needles:

The first reaction represents the dehydration of the material.

$$Wet - Pine \xrightarrow{w_1} Dry - Pine + H_2O$$

The reactions under nitrogen are:

$$Dry - Pine \xrightarrow{\dot{w}_2} \nu_1(\alpha - Pine) + (1-\nu_1)\,gas$$
$$\alpha - Pine \xrightarrow{\dot{w}_3} \nu_2(\beta - Pine) + (1-\nu_2)\,gas$$
$$\beta - Pine \xrightarrow{\dot{w}_4} \nu_3 Char + (1-\nu_3)\,gas$$

While the reactions under air are:

$$\alpha - Pine \xrightarrow{\dot{w}_5} \nu_4(\beta - Pine) + (1-\nu_4)\,gas$$
$$\beta - Pine \xrightarrow{\dot{w}_6} \nu_5 Char + (1-\nu_5)\,gas$$
$$Char \xrightarrow{\dot{w}_7} \nu_6 residue + (1-\nu_6)\,gas$$

Notice that generic names are used to describe the intermediate phases. The thermal degradation reactions can be written as follows (Figure 11):

From the proposed mechanism, a model is developed with a view to represent the thermal decomposition of the pine needles in 0-Dimension, based on the TGA experiments. This kind of model represents the thermal degradation with negligible gradients of temperature and species as

occurring in an ideal thermo-gravimetric experiment. It means that the model 0-Dimension accounts for only the kinetics of thermal degradation of the pine needles.

d) Estimation of the kinetic parameters

This section presents the modelling of the results obtained from TGA experiments (mg scale) by using the mechanism of the thermal degradation proposed previously in Figure 11. The modelling is based on each step of the mechanism that corresponds to a reaction described by a modified Arrhenius law by following previous reports [11, 19]:

$$\dot{\omega}_1 = A e^{-E/RT} m_i^n y_{O2}{}^{\delta}$$

Where: A is the pre-exponential factor, Ea the activation energy, n the reaction order, v the stoichiometric factor and y_{O2} the mass fraction of oxygen. Notice that δ is 1 under air and 0 under nitrogen.

The total mass loss rate of the solid is then described as the sum of the mass loss rate of each of the product in the condensed phase:

$$\frac{dm}{dt} = \Sigma MLR = \frac{dm_{pine}}{dt} + \frac{dm_{\alpha}}{dt} + \frac{dm_{\beta}}{dt} + \frac{dm_{Char}}{dt} + \frac{dm_{\mathrm{Re}\,sidue}}{dt}$$

Or:

$$\frac{dm}{dt} = -\left((1-\nu_1)\cdot\omega_1 + (1-\nu_2)\cdot\omega_2 + (1-\nu_3)\cdot\omega_3 + (1-\nu_4)\cdot\omega_4 + (1-\nu_5)\cdot\omega_5 + (1-\nu_6)\cdot\omega_6\right)$$

The kinetic constants of the Arrhenius law for each reaction, as well as the stoichiometric parameters, need to be estimated as these parameters cannot be measured or determined experimentally. In practice, a Genetic Algorithm (GA) method has been used to estimate the kinetic parameters as reported in the past [9-10]. This method aims to extract the material properties needed for the numerical model from laboratory experiments like cone calorimeter and TGA [9-10]. In fact, the (GA) method used to find a set of material properties that offer optimal agreement between the numerical model and the experimental data, in accordance to the constraints imposed by the model and the experiments [9-10]. This method has been reported in

detail elsewhere [9-10, 19-20]. The kinetic parameters are calculated in two steps. First, the parameters corresponding to the thermal degradation under nitrogen are determined.

In a second step, those parameters are considered constant and then the calculation of the parameters of the reactions under air is done. The values calculated for these parameters are presented in the Table 3.

In order to complete the model input, the process of dehydration of the pine has also been included. This step is widely reported [19-20], but has not been utilized specifically, as in the context of the present work. The parameters founded in [19] were inserted directly in the present model. Table 4 presents the kinetic parameters of the dehydration reaction.

Figures 12 and 13 present the comparison between the experimental and numerical results regarding the evolution of the mass loss rate under nitrogen and air, respectively, for the different heating rates. As can be seen, the numerical MLR evolutions show a good agreement with the experimental results, for all heating rates and under both atmosphere conditions. Therefore, the proposed model clearly validates the experimental data in the case of TGA runs (0-Dimension).

3.2.Cone calorimetric analysis

Experiments in TGA have shown the thermal degradation behaviours of pine needle samples. A mechanism has also been suggested by analysing mass loss, mass loss rate and gaseous emissions under different heating rates. However, in this type of experiments, the sample sizes are relatively very small and are therefore considered to be thermally thin. As a consequence, no gradients of temperature are assumed with in the sample. With a view to obtaining a better picture of the combustion profiles of the sample and to understand the heat and mass transfers pertaining to a porous bed of sample, cone calorimetric runs were done. The results are presented below.

Ignition of solid fuels has been extensively explored providing “the classical theory of ignition” as detailed in a previous report [39]. Here, two cases were identified. The first one examines thin objects having no spatial and internal temperature gradients. This is named as a thermally thin case. The second one, named as a thermally thick case, incorporates temperature gradients into

the solid fuel bed. In general, fuels are classified as thermally thin if the Biot number is much smaller than 0.1, here the Biot number [40] defined as follows (equation 5):

$$Bi = \frac{\dot{q}_e^{"}}{k\sigma\left(T_{ig} - T_{\infty}\right)} \qquad (5)$$

The calculation has been reported in a previous work [41]. For the range of heat fluxes tested, the Biot number varied from 7.4e-05 to 2.46e-04, corresponding to a thermally thin material.

However, Figure 14 presents the inverse of the square root of the ignition delay, t_{ig} and the inverse of the ignition delay t_{ig} as functions of the external heat flux. The evolution of the inverse of the square root of t_{ig}, shows a better linearity than that for the inverse of t_{ig}. Even though single pine needles are expected to behave as a thermally thin material during cone calorimeter experiments, the porous bed of pine needles behaves like a thermally thick sample.

Moreover, Figures 15 and 16 show the evolution of temperatures with time at the centreline of the sample for two external heat fluxes, 15 $kW.m^{-2}$ and 50 $kW.m^{-2}$, respectively. For the lowest external heat flux, the bed of pine needles behaves like in accordance to a pure conduction model before the ignition. However, in this case, we need to consider the radiation effects that appear in depth due to the high porosity of the bed in addition to the conduction mode of heat transfer. But in actual practice, the two heat transfer processes could be treated as one and the effective parameters of the solid could be derived, such as, effective conductivity, effective heat capacity, etc. [21, 28, 40].

The temperatures near the back surface of the sample (V3, V4, and V5) were found to be higher than those near the surface exposed to the heat flux. This can be attributed to the oxidative reactions in the condensed phase and other reactions in gas phase owing to porosity of the sample. Both these reactions are exothermic in nature and thus result in an overall rise of temperature of the sample. It should be noted here that the back surface of the sample thus preventing any substantial thermal losses.

The temperatures near the surface of the sample are also affected by the convective heat transfer. It is one of the reasons that these temperatures are lower than those found deeper in the bed. For

a heat flux of 50 kW.m^{-2}, we can observe that the temperature gradients along the centreline of the sample are lower than the corresponding ones under the lower irradiance level (i.e. at 15 kW/m²).

In the following sections the mass loss rate evolution and the gaseous emissions during the degradation process in the cone calorimeter apparatus, under well ventilated atmosphere, and a compilation of the cone calorimeter output are presented. Figure 17 presents the evolution of the mass loss rate as a function of the time, at 15, 20, 30, 40 and 50 kW.m^{-2} (here time t=0 is taken as the beginning of the exposure to the irradiance level). These curves show similar evolutions at 15, 20 and 30 kW.m^{-2}, after which the value of the MLR becomes more prominent with the increase of the heat flux; however, the duration of the degradation becomes less important.

At 15, 20 and 30kW.m^{-2}, the MLR curves show two peaks, first one occurs at 200, 60 and 25 sec and the second one occurs at 225, 80 and 40 sec, respectively (the delays to ignition are reported in the table 2; no ignition has been observed under 12 kW.m^{-2}, thus $CHF_{experimental}$ is 12 kW.m^{-2}). The first sets of peaks are attributed to the thermal degradation of a thin surface in the bed. The second one is due to pyrolytic reactions if the pine needles that are in the bed. After the second peak, the intensity of MLR decreases slightly until the end of the test, and this stage is related to the char oxidation.

At higher heat fluxes, 40 and 50 kW.m^{-2}, one main peak was observed and then the intensity of MLR decreases slightly. In this case the combustion of the bed occurs in a full blown manner and no separation of a pyrolysis zone and a virgin fuel zone was observed. Indeed, related to the evolution of temperatures (figures 15 and 16), the temperature gradients were found to be small and when ignition occurred, the bed burned through its entire depth.

Heat release rate (HRR) of a burning fuel is a very important parameter for understanding the intensity of its combustion process, the fire characteristics and propagation rates [33]. It also serves to define parameters such as flame geometry, temperature fields, rate of fire growth and the amount of smoke and toxic gas generated. Oxygen consumption measurement [32] is a convenient and widely used technique to determine the heat release rate for the cone calorimeter apparatus, as described in the standard ISO 5660 [17]. HRR is calculated from the amount of O_2

consumed during a combustion process [32], based on the fact that for a large number of fuels, the energy released per unit of mass of oxygen consumed can be considered as the Huggett's constant (E), which is equal to 13.1 MJ.kg^{-1}. In general, several simplifying assumptions are made: all exhaust gases are considered to behave as ideal, and to be composed (for more than 99%) only of O_2, CO_2, CO, H_2O and nitric oxide species [42-46].

As H_2O vapour concentrations were measured during our experiments, the HRR values were computed using the following equation (6) (described in details in reference [32, 46]):

$$HRR = \frac{1}{A}\left[E\phi - (E_{CO} - E)\frac{1-\phi}{2}\frac{X_{CO}}{X_{O_2}}\right]\frac{M_{O_2}}{M_{Air}}\dot{m}_{Air}\left(1 - X^0_{H_2O} - X^0_{CO_2}\right)X^0_{O_2} \quad (6)$$

Where, A = 88.4 cm^2 (sample area exposed to cone calorimeter heat flux), E = 13.1 MJ kg^{-1} of O_2, E_{CO} = 17.6 MJ kg^{-1} of O_2, M_{O2} = 32 g mol^{-1}, M_{Air} = 29 g mol^{-1}, X_i is the mole fraction of species *i* in the exhaust gas (measured by the analysers), X_i^0 is the mole fraction of species *i* in the incoming air. The oxygen depletion factor (ϕ) is defined in detailed in [42] and hence it is not presented here.

Figure 18 shows the transient evolution of the heat release rate (HRR) at the five irradiance levels (15, 20, 30, 40 and 50 kW.m^{-2}) studied. As shown previously for MLR, HRR transient evolutions depend strongly on the irradiance level, and profiles of both parameters have the same shape compared to MLR one for a given external heat flux. It can be also noticed that higher the heat flux and higher is the intensity of HRR. The values here obtained are in accordance with those already found in the literature [37].

During the experiments, the cone calorimeter apparatus was coupled with two kinds of gas analysers: a Horiba PG 250 and a FTIR apparatus. The oxygen content (O_2) of ambient air and concentrations of fifteen gaseous combustion products were continuously tracked and measured, and they included: CO, CO_2, NO, NO_2, SO_2, NH_3, HCN, N_2O, CH_4, C_2H_2, C_2H_4, C_2H_6, C_3H_6, C_3H_8 and H_2O. HCN and some lightweight hydrocarbons (C_2H_2 and C_2H_4) were observed during these experiments in very low concentrations, so their evolutions are not considered here. In fact the major gases emitted during the experiments were: CH_4, CO, CO_2, NO and H_2O vapour.

The evolutions of concentrations of the major emissions correlated with the MLR at 30 kW m^{-2} are plotted in figure 19. It should be also noted here that the emissions obtained at this specific irradiance level are representative of the corresponding ones for the other heat fluxes. In addition to monitoring and measuring the main gas species (CH_4, CO, CO_2, NO and H_2O vapour), the residual oxygen concentration in the smoke layer was also followed.

The FTIR analysis technique used included sampling and filtering devices that were validated during the SAFIR project [43], which also constituted the basis for toxicity analysis carried out following the guidelines of the standard ISO 19702 [44-45]; this technique has been used in previous works [41, 46-49]. Based on visual observations, the main features of the experiments can be classified into the following groups (see also Table 6):

- From the beginning of test and the ignition: this step starts with the rise of solid‘s temperature without production of any gas (i.e. originating owing to the thermal mass or thermal inertia of the materials). Notice that a glowing glare was observed visually for the lower heat fluxes.

  Just before the flaming combustion, gases can be seen released from the sample, the quantity of gases was found to increase with the time until ignition. In general, a small mass loss was also observed and only water vapour and methane were detected during this step.

- Combustion phase: The flame covers the whole of the pine needles bed, and it regresses gradually with the time. At this stage, CO_2, CO, H_2O, CH_4 NO were detected and around 10.5 g of the mass was lost during this step.
- Oxidation phase: after the flameout, some quantity of the solid remained in the sample holder, and the quantity of gases produced was negligible. Only methane and CO and CO_2 were detected during this step.

In short, the thermal degradation and combustion of the pine needles in the cone calorimeter apparatus can be considered to occur via the following steps:

- During the very initial stages (especially at lower heat fluxes), the mass loss rate is related to the removal of moisture.
- During the very initial stages, removal of moisture primarily causes the MLR as is observed at relatively lower heat fluxes,
- In the second step, emission of NO is observed, whose concentration increases as the heat fluxes rise.
- Next, the flaming combustion sets in leading to the consumption of oxygen and the production of CO_2 and H_2O.
- After the peak stage of the above step, CO is produced and the concentration of O_2 increases in an inverse manner.
- Finally, after the flame out, the MLR continues to decrease slowly with the generation of CO and CH_4.

Conclusions

In the present work, the thermal degradation of the pine needle was investigated at two different scales, using a TGA and cone calorimeter. At smaller scale, the experiments were carried out at four heating rates, under two atmospheres (air and N_2) in a TGA apparatus. The mass loss, the mass loss rate and the gaseous emissions were measured for the material as a function of the temperature. From the profiles of the mass loss, mass loss rate and gaseous emissions under air and nitrogen, a model is proposed for the thermal degradation which incorporates the following steps:

- A four steps mechanism in nitrogen atmosphere.
- A three steps additional mechanism under air.

The kinetic parameters were estimated using a genetic algorithm method. The model developed was for heating rates under both atmospheres. Generally a good agreement was obtained between the experimental and numerical mass loss rate evolutions. Furthermore, the influence of the atmosphere on the different reactions steps was also identified.

At the larger scale, the experiments were conducted by using a cone calorimeter at five different values of heat flux. The mass loss, mass loss rate, and the evolution of vertical temperature profiles in the fuel bed and the gaseous emissions were monitored.

The results show that the bed of pine needles behaves as a thermally thick fuel. However, at higher the external heat fluxes, fuel bed showed an increasing propensity to behave like a thermally thin sample.

Furthermore, HCN and other lower hydrocarbons (C_2H_2 and C_2H_4) were observed during these experiments, but only in very low concentrations, so their evolutions were not shown graphically. In practice, the major gaseous components included CH_4, CO, CO_2, NO and H_2O. As the cone calorimetric runs were performed in ambient conditions (i.e. at an oxygen concentration of 21 vol.%), which in fact is much higher compared to that available in actual fire scenarios, it is highly desirable to repeat the study under different intermediates concentrations of oxygen. Finally, the results obtained in the actual investigation can be used as input data to model the thermal decomposition of ligno-cellulosic materials in cone calorimeter experiments by using different available methods.

Acknowledgments

The authors wish to thank the “Institut des Risques Industriels Assurantiels et Financiers” for its technical and human support into the Hestia Platform. This work pertains to the French Government program “Investissements d’Avenir” (LABEX INTERACTIFS, reference ANR-11-LABX-0017-01).

REFERENCES

1. Alexandrian, D., Esnault, F., Calabri, G., Forest fires in the Mediterranean area, FAO meeting on Public Policies Affecting Forest Fires. (1998) Rome Italy.
2. McArthur, A.G., Weather and grassland fire behaviour. Department of National Development, Forestry and Timber Bureau Leaflet No. 100. (1966) Canberra, Australia.

3. Turner, J.A., Lawson, B.D., Weather in the Canadian Forest Fire Danger Rating System. A user guide to national standards and practices. Victoria, British Columbia: Environment Canada, (1978).
4. Rothermel, R.C., A mathematical model for predicting fire spread in wildland fuels. Res. Pap. INT-115. Ogden, UT: U.S. Department of Agriculture, Forest Service, Intermountain Forest and Range Experiment Station (1972).
5. Rhodes, B.T., Quintiere, J.G., Burning rate and flame heat flux for PMMA in a cone calorimeter, Fire safety Journal. 26 (1996) 221-240.
6. ASTM E1321, Standard method for determining material ignition and flame spread properties.
7. Delichatsios, M.A., Chen, Y., Asymptotic, approximate and numerical solutions for the heat-up and pyrolysis of materials including re-radiation losses, Combustion and Flame. 92 (1993) 292-307.
8. Cancellieri, D., Innocenti, E., Leroy-Cancellieri, V. WinGPYRO: A software platform for kinetic study of forest fuels. Fire safety journal. 58 (2013) 103-111.
9. Rein, G., Lautenberger, C., Fernandez-Pello, C., Torero, J., Urban, D., Application of genetic algorithms and thermogravimetry to determine the kinetics of polyurethane foam in smoldering combustion, Combustion and Flame. 146 (2006) 95-108.
10. Lautenberger, C., Rein, G., Fernandez-Pello, C., The application of a genetic algorithm to estimate material properties for fire modeling from bench scale Fire test data, Fire Safety Journal. 41 (2006) 204-214.
11. Di Blasi, C., Modeling chemical and physical processes of wood and biomass pyrolysis, Progress in Energy and Combustion Sciences. 34 (2008) 47–90.
12. Fateh, T., Rogaume, T., Luche, J., Richard F., Jabouille, F., Kinetic and mechanism of the thermal degradation of a plywood by using thermogravimetry and Fourier-transformed infrared spectroscopy analysis in nitrogen and air atmosphere, Fire Safety Journal. 58 (2013) 25-37.
13. Wilkie, C.A., TGA-FTIR an extremely useful technique for studying polymer degradation, Polymer Degradation and Stability. 66 (1999) 301–306.

14. Mehrabian, R., Scharler, R., Obernberger, I., Effects of pyrolysis conditions on the heating rate in biomass particles and applicability of TGA kinetic parameters in particle thermal conversion modeling, Fuel. 90 (2012) 567-575.
15. Chuang, F.S., Analysis of thermal degradation of diacetylene-containing polyurethane copolymers, Polymer Degradation and Stability. 92 (2007) 1393-1407.
16. Richard, W.C., Mark A.S., Quantitative flash pyrolysis Fourier transforms infrared spectroscopy of organic materials, Analytica Chimica Acta**.** 639 (2009) 62-66.
17. ISO 5660. Fire test Reaction to fire, rate of heat release from building products, ISO, Geneva (1993).
18. Delichatsios, M.A., Piloted ignition times, critical heat fluxes and mass loss rates at reduced oxygen atmospheres, Fire Safety Journal. 40 (2005) 197–212.
19. Lautenberger, C., Fernandez-Pello, C., A model for the oxidative pyrolysis of wood.Combustion and Flame. 156 (2009) 1503-1513.
20. Lautenberger, C., Fernandez-Pello, C., Generalized pyrolysis model for combustible solids, Fire Safety Journal. 44 (2009) 819-839.
21. Mindykowski, P., Fuentes, A., Consalvi, J.L., Porterie, B., Piloted ignition of wildland fuels, Fire safety Journal 46 (2011) 34-40.
22. Safi, M., Mishra, I., Prasad, B., Global degradation kinetics of pine needles in air, Thermochimica Acta. 412 (2004) 155-162.
23. Simeoni, A., Thomas, J., Bartoli, P., Borowieck, P., Reszka, P., Colella, F., Santoni, P., Torero, J., Flammability studies for wildland and wildland–urban interface fires applied to pine needles and solid polymers, Fire Safety Journal. 54 (2012) 203-217.
24. Battye, W., Battye, R., Development of Emissions Inventory Methods for Wild-land Fire, Final Report. EPA Contract No. 68-D-98-046. Research Triangle Park, NC: US Environmental Protection Agency. 82 s, 2002.
25. Rein, G., Torero, J., Guijarro, M., Esko, M., Castro. A., D2.1-1 Methods for the experimental study and recommendations for the modelling of pyrolysis and combustion of forest fuels. Fire paradox, 2008.
26. Jervis, F., Rein, G., Experimental study on the burning behaviour of Pinus halepensis needles using small-scale fire calorimetry of live, aged and dead samples, Fire And Materials. Article first published online: 3 FEB 2015 DOI: 10.1002/fam.2293.

27. Shen, D., Gu, S., Jin, B., Fang, M., Thermal degradation mechanisms of wood under inert and oxidative environments using DAEM methods, Bioresource Technology. 102 (2011) 2047-2052.
28. Zaida, J., Étude expérimentale et numérique de la dégradation thermique des lits combustibles végétaux, Ph.D Thesis, Ouagadougou University (2012).
29. Pimont, F., Dupuy, J.L., Caraglio, Y., Morvan, D., Effect of Vegetation Heterogeneity on Radiative Transfer in Frest Fires, International Journal of Wildland Fire. 18 (2009) 536-553.
30. Torero, J.L., Flaming ignition of solid fuels, The SFPE handbook of fire protection engineering 4th Edition, chapter 11, page 2-262.
31. Fateh, T., Etude expérimentale et numérique de la cinétique de décomposition thermique de contre plaqués en bois, Ph.D Thesis, Poitiers University (2011).
32. Bustamante Valencia, L., Rogaume, T., Guillaume, E., Rein, G., Torero, J., Analysis of principal gas products during combustion of polyether polyurethane foam at different irradiance levels, Fire Safety Journal. 7 (2009) 933-940.
33. Babrauskas, V., Development of the cone calorimeter, a bench-scale heat release rate apparatus based on oxygen consumption, Fire and Materials. 8 (1983) 81-95.
34. Yorulmaz, S.Y., Atimtay, A.T., Investigation of combustion kinetics of treated and untreated waste wood samples with thermogravimetric analysis, Fuel Processing Technology. 90 (2009) 939-946.
35. White, R.H., Dietenberger, M.A., Wood products: thermal degradation and fire, Encyclopedia Materials. (2001) 9712–9716.
36. Sonibare, O., Ehinola, O., Egashira, R., Kean Giap, L., An investigation into the thermal decomposition of Nigerian coal, Journal of Applied Sciences. 5 (2005) 104–107.
37. Bartoli, P., Simeoni, A., Biteau, H., Torero, J.L., Santoni, P.A., Determination of the main parameters influencing forest fuel combustion dynamics, Fire safety Journal. 46 (2011) 27-33.
38. Fernandez-Gomez, I., de Castro, A.J., Guijarro, M., Madrigal, J., Aranda, J.M., Diez, C., Hernando, C., Lopez, F., Characterization of forest fuels in a Mass loss calorimeter by short open-path FTIR spectroscopy. Journal of Quantitative Spectroscopy and Radiative Transfer. 112 (2011) 519–530.

39. Quintiere, J., A semi-quantitative model for the burning rate of solid materials. NISTIR 4840, National Institute of Standards and Technology, Gaithersburg, MD, 1992.
40. Benkousas, B., Consalvi, J.L., Porterie, B., Sardoy, N., Loraud, J.C., Modelling thermal degradation of woody fuel particles, International Journal of Thermal Sciences. 46 (2007) 319-327.
41. Fateh, T., Richard, F., Batiot, B., Rogaume, T., Luche, J., Zaida, J., Characterization of the burning behavior and gaseous emissions of pine needles in a cone calorimeter – FTIR apparatus, Fire Safety Journal. 82 (2016) 91-100.
42. Janssens, M. L., Measuring Rate of Heat Release by Oxygen Consumption, Fire technology 27 (1991) 234 – 249.
43. Hakkarainen, T., et Al. Smoke Gas Analysis by Fourier Transform Infrared Spectroscopy, The SAFIR Project, European commission research program contract number SMT 4-CT96-2136 - Technical Research Centre of Finland, Copyright Valtron Teknillinen Tutkimuskesus, 1999. http://www.vtt.fi/rte/firetech/research/html Smoke analysis by Fourier transform infra-red spectroscopy (SAFIR).
44. ISO 19702. Toxicity testing of fire effluents – Guidance for analysis of gases and vapours in fire effluents using FTIR gas analysis. ISC 13.220.01.
45. Fardell, P., Guillaume, E., Sampling and measurement of toxic fire effluents, Fire Toxicity. Chapter 11, 2010.
46. Luche, J., Rogaume, T., Richard, F., Guillaume, E., Characterization of Thermal Properties and Analysis of Combustion Behaviour of PMMA in a Cone Calorimeter, Fire Safety Journal. 46 (2011) 451-461.
47. Fateh, T., Rogaume, T., Luche, J., Richard, F., Jabouille, F., Characterization of the thermal decomposition of two kinds of plywood with a cone calorimeter – FTIR apparatus, Journal of Analytical and Applied Pyrolysis. 107 (2014) 87-100.
48. Fateh, T., Rogaume, T., Richard, F., Multi-scale modeling of the thermal decomposition of fire retardant plywood, Fire Safety Journal. 64 (2014) 36-47.
49. Fateh, T., Richard, F., Rogaume, T., Joseph, P., Experimental and modelling studies on the kinetics and mechanisms of thermal degradation of polymethyl methacrylate in nitrogen and air, Journal of Analytical and Applied Pyrolysis. 120 (423-433).

Table 1: Comparison between the Mass fractions for different kind of fuels.

	Mass fraction								
Fuel	**Cellulose (%)**	**Lignin (%)**	**Holocellulose (%)**	**Hemicellulose (%)**	**Extractible (%)**	**C (%)**	**H (%)**	**O (%)**	**N, Mineral (%)**
AU	38.0	41.6	43.2	5.2	13.1	48.3	6.2	40.3	5.3
EA	40.7	39.7	54.3	13.6	5.8	52.4	7.0	35.9	4.6
CM	39.4	34.4	52.0	12.6	9.2	46.6	6.2	37.7	9.5
PP	38.3	28.9	42.4	5.1	12.9	46.9	6.0	39.6	1.0

Table 2. Pine Needles decomposition taking into accounts the evolution of solid and gas phases.

No.	Type of reaction	Range of temp.[°C]	Condensed reagent	Condensed products generated	Gaseous products emitted
1	Drying		Wet-Pine	Dry-Pine	H_2O
2	Pyrolysis	200-330°C	Dry-Pine	α-Pine	CO_2, Acetic acid, Formic acid, CH_3OH, H_2O.
3	Pyrolysis	330-420°C	α-Pine	β-Pine	CO_2, Acetic acid, Formic acid, H_2O, CO.
4	Pyrolysis	> 420°C	β-Pine	Char	H_2O, CH_4, Alkyl, CO_2, CO.
5	Oxidation	280-330°C	α-Pine	β-Pine	CO, H_2O, NH_3, Acetic acid, Formic acid.
6	Oxidation	330-420°C	β-Pine	Char	CO, NH_3, H_2O, CO_2.
7	Oxidation	>420°C	Char	Residue	H_2O, CH_4, CO, CO_2

Table 3. Kinetic parameters values estimated by using GA for the kinetic of thermal decomposition of pine needles.

Atmosphere	Reagent	Product	Kinetic parameters values			
			$Log_{A\ (S^{-1})}$	$E_{a\ (kJ.mol^{-1})}$	n(–)	v(–)
N_2	Pine (dry)	α-Pine	6.5	91	1	0.85
N_2	α-Pine	β- Pine	7.1	110	0.9	0.66
N_2	β- Pine	char	5.2	95	2.3	0.58
Air	α- Pine	β- Pine	7.5	115	1.3	0.26
Air	β- Pine	char	8.2	89	2.8	0.49
Air	Char	Residue	7.5	128	0.9	0.05

Table 4: Kinetic parameters of dehydration of the pine needles.

$\log_{10}A(s^{-1})$	E ($kJ.mol^{-1}$)	n (–)	v(–)
3.6	43.8	0.99	0.9

Table 5. Synthesis of the average results as a function of the external heat flux.

External heat flux	**Piloted ignition**	**Flame Out**	**PHRR**	**MLR (Max)**
($kW.m^{-2}$)	t_{ig} (Sec)	t_{ig} (Sec)	($kW.m^{-2}$)	($g.s^{-1}$)
15	209.5±65.5	304.5±51.5	238	0.29
20	68±5	158±6	240	0.27
30	20.5±2.5	117±2.3	275	0.31
40	12±2	108±6	320	0.43
50	7.5±0.5	105±2	325	0.57

Table 6: A synthesis of the Gaseous products emitted and Total Mass loss during the experiments.

	Before Ignition	ignition	After flame out
Gaseous products emitted	H_2O, CH_4.	CO_2, CO, H_2O, CH_4, NO	CH_4, CO, CO_2
TML (g)	1.2	10.5	2.5

Figure 1: The sample holder used in the present study.

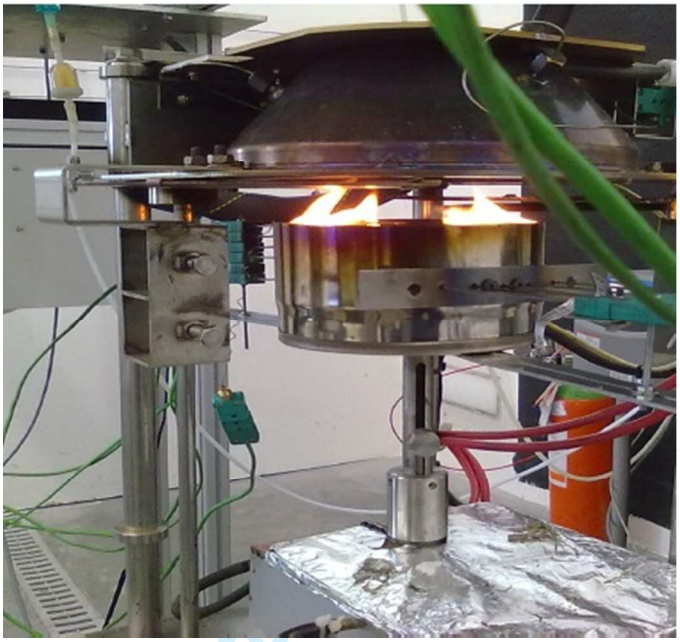

Figure 2: Position of the thermocouples positioning along the centerline of the sample holder.

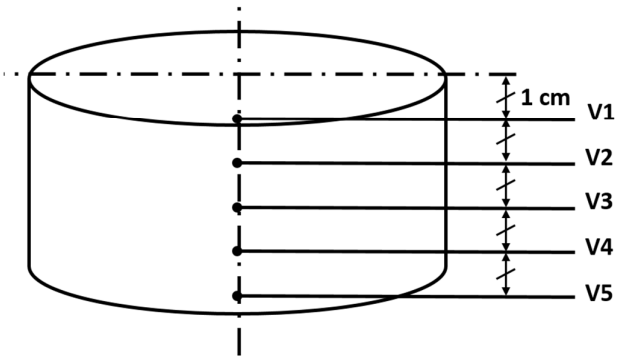

Figure 3: Evolution of the mass loss as a function of the temperature in TGA under inert atmosphere.

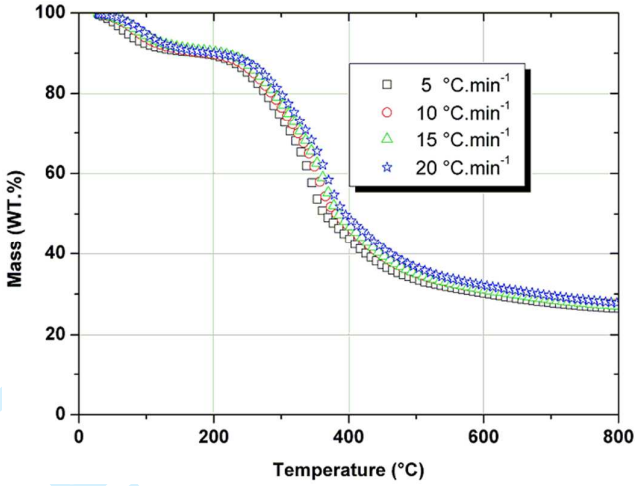

Figure 4: Evolution of the mass loss rate as a function of the temperature in TGA under inert atmosphere.

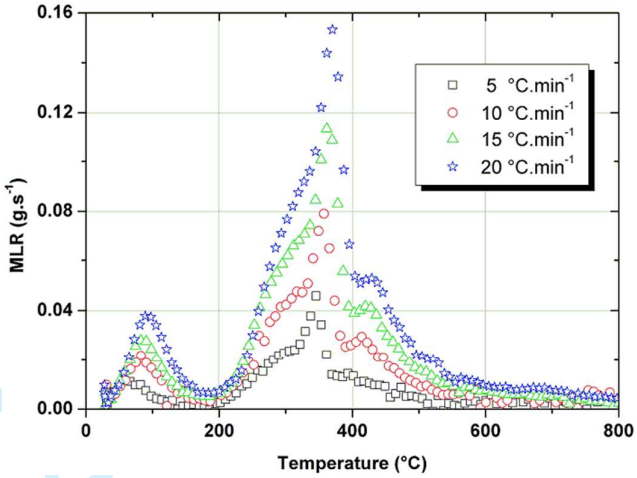

Figure 5: Evolution of the gaseous emissions and the MLR under N_2 in TGA at 10°C min^{-1}.

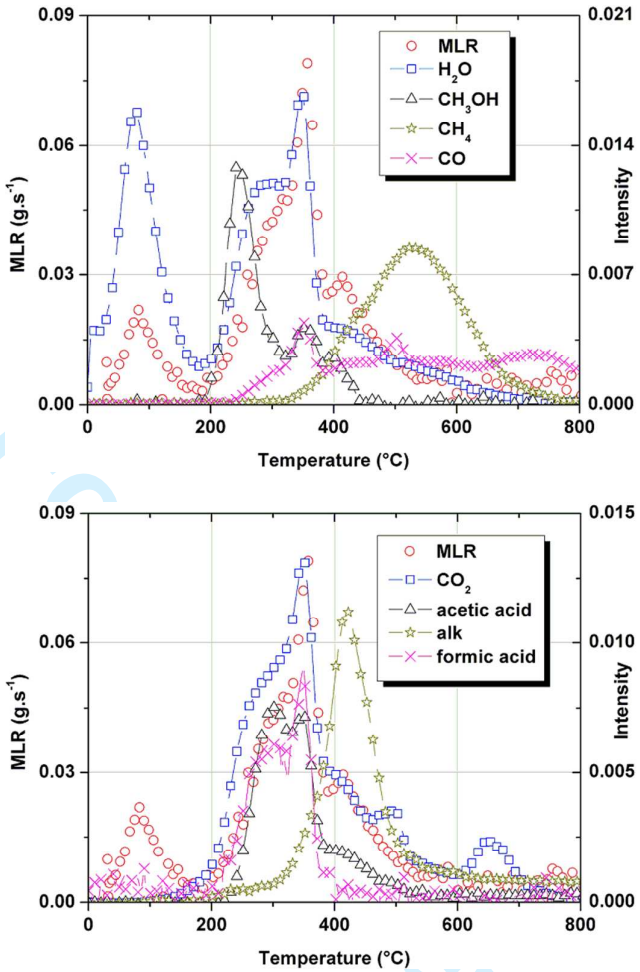

Figure 6: Evolution of the mass loss as a function of the temperature under air in TGA.

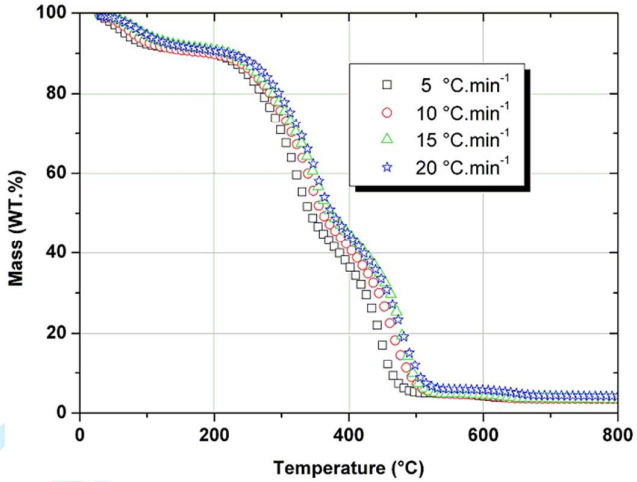

Figure 7: Evolution of the mass loss rate as a function of the temperature under air in TGA.

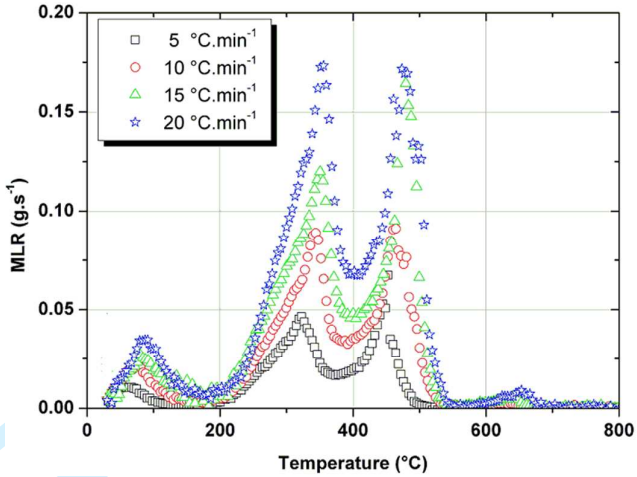

Figure 8: Evolution of the gaseous emissions and the MLR under air in TGA at 10°C min^{-1}.

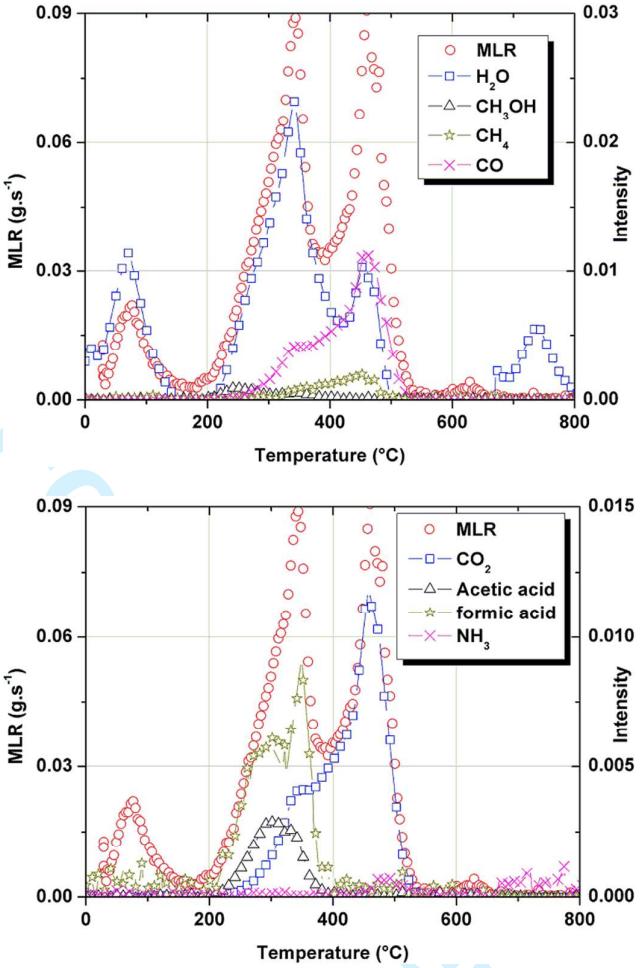

Figure 9: Comparison of the evolution of the mass under nitrogen and under air in TGA for a heating rate of 10°C min^{-1}.

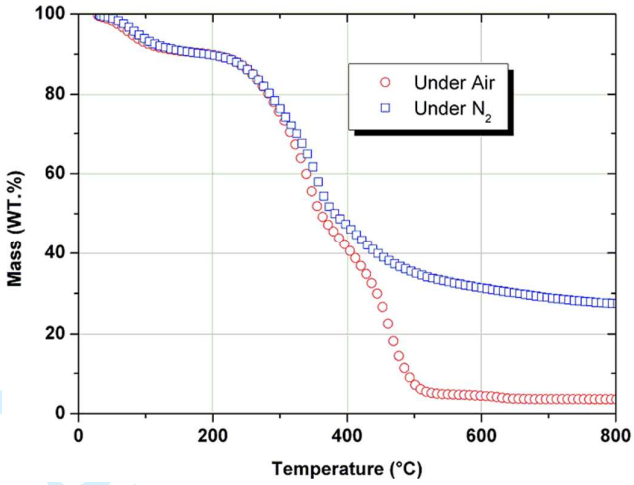

Figure 10: Comparison of the evolution of the mass under nitrogen and under air in TGA for a heating rate of 10°C min^{-1}.

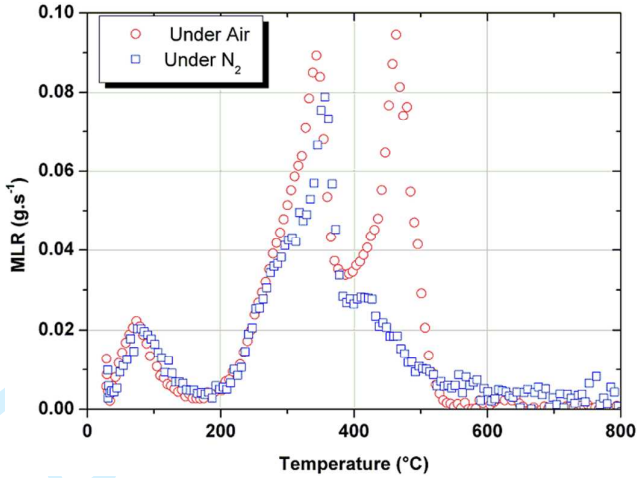

Figure 11: Mechanism proposed for the thermal degradation.

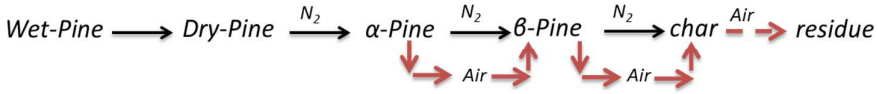

Figure 12: Comparison of the experimental and modeled MLR under inert atmosphere in 0-D.

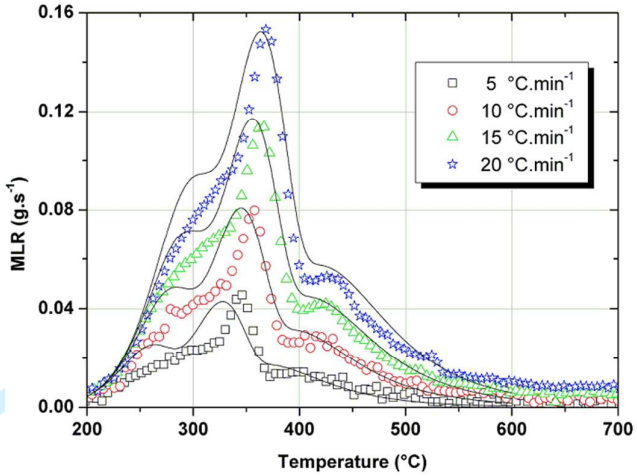

Figure 13: Comparison of the experimental and modeled MLR under air in 0-D.

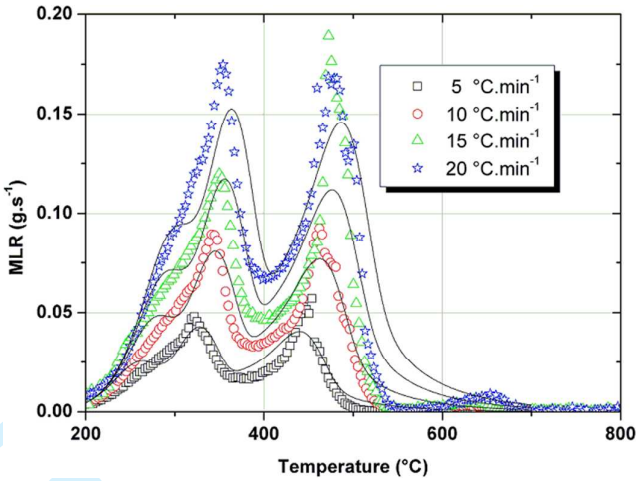

Figure 14: Plots of the inverse of the square root of t_{ig} and of the inverse of t_{ig}.

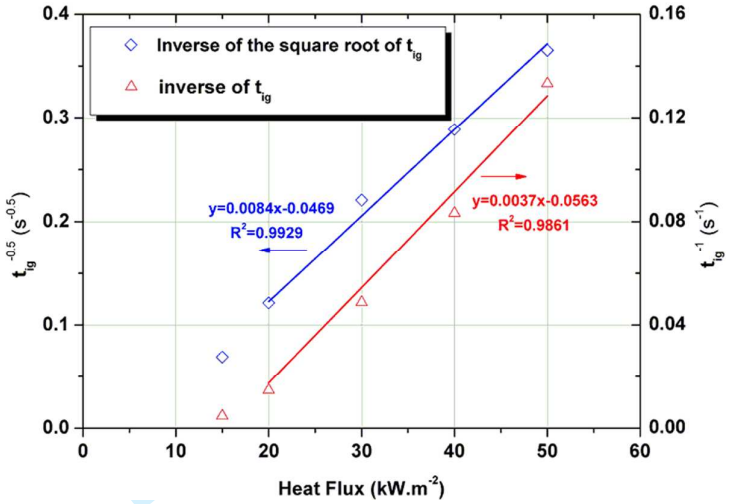

Figure 15: Evolution of the temperatures (vertical position) at 15 kW.m^{-2}.

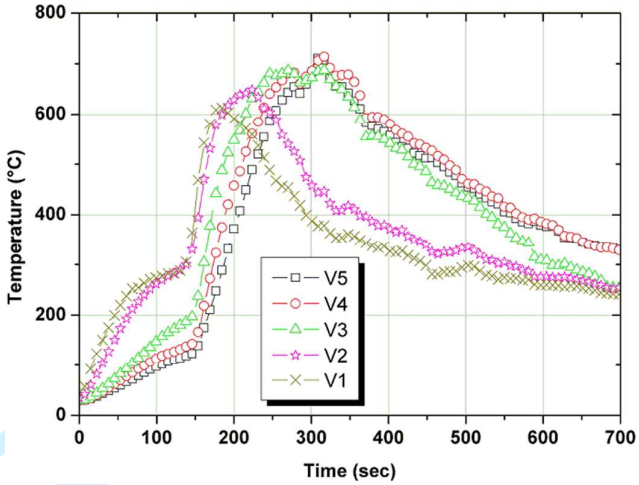

Figure 16: Evolution of the temperatures (vertical position) at 50kW.m^{-2}.

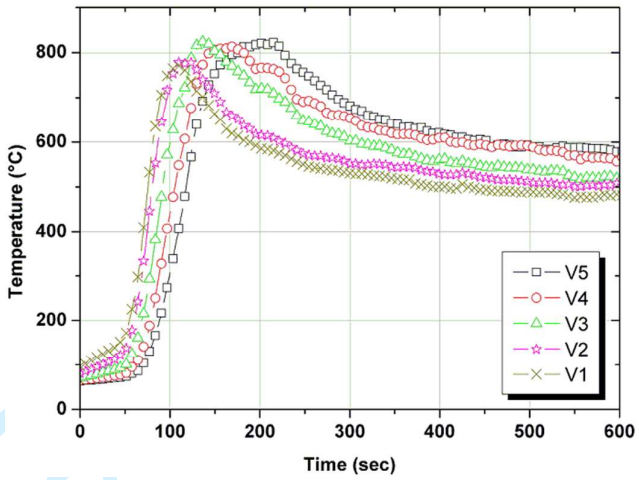

Figure 17: Evolution of the mass loss rate as a function of the time in the cone calorimeter.

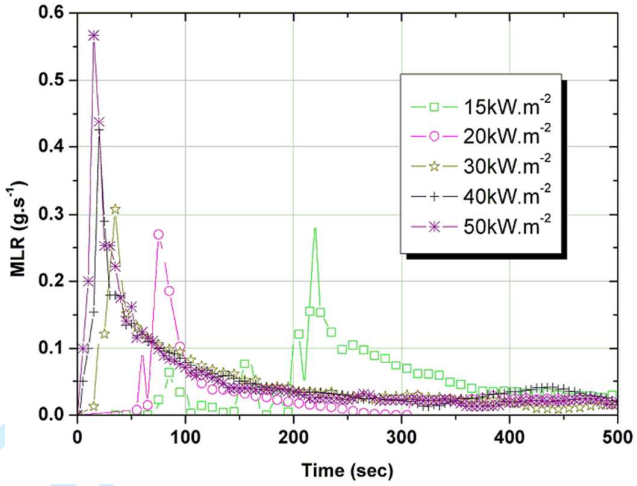

Figure 18: Evolutions of the HRR as a function of time for the different external heat fluxes.

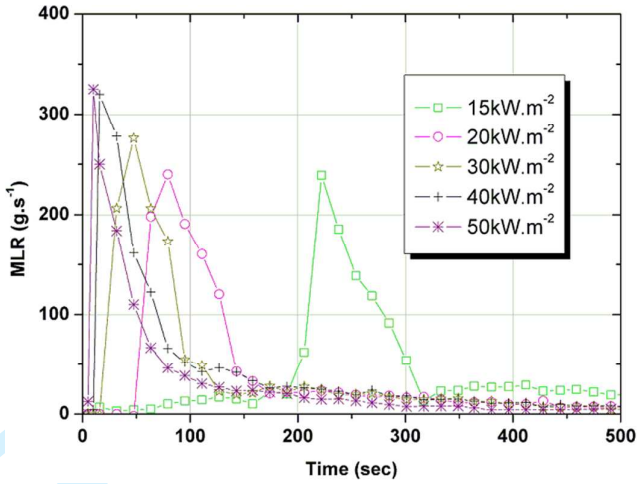

Figure 19: Evolution of the gaseous emissions during the experiment at 30 kW m^{-2} (CH_4*100, CO*10, CO_2, NO*100, H_2O, MLR*10000, O_2).